

Article

Photocatalytic Decomposition of Nitrobenzene in Aqueous Solution by Ag/Cu₂O Assisted with Persulfate under Visible Light Irradiation

Wen-Shing Chen * and Jyun-Yang Chen

Department of Chemical and Materials Engineering, National Yunlin University of Science & Technology, 123 University Road, Section 3, Douliou 640, Yunlin, Taiwan; m10915009@yuntech.edu.tw

* Correspondence: chenwen@yuntech.edu.tw; Tel.: +88-6553-42601 (ext. 4624); Fax: +88-6553-12071

Abstract: The mineralization of nitrobenzene was executed using an innovative method, wherein Ag/Cu₂O semiconductors stimulated by visible light irradiation were supported with persulfate anions. Batch-wise experiments were performed for the evaluation of effects of silver metal contents impregnated, persulfate concentrations and Ag/Cu₂O dosages on the nitrobenzene removal efficiency. The physicochemical properties of fresh and reacted Ag/Cu₂O were illustrated by X-ray diffraction analyses, FE-SEM images, EDS Mapping analyses, UV-Vis diffuse reflectance spectra, transient photocurrent analyses and X-ray photoelectron spectra, respectively. Because of intense scavenging effects caused by benzene, 1-propanol and methanol individually, the predominant oxidant was considered to be sulfate radicals, originated from persulfate anions via the photocatalysis of Ag/Cu₂O. As regards oxidation pathways, nitrobenzene was initially transformed into hydroxycyclohexadienyl radicals, followed with the production of 2-nitrophenol, 3-nitrophenol or 4-nitrophenol. Afterwards, phenol compounds descended from denitration of nitrophenols were converted into hydroquinone and *p*-benzoquinone.

Keywords: nitrobenzene; Ag/Cu₂O; persulfate; sulfate radical



Citation: Chen, W.-S.; Chen, J.-Y. Photocatalytic Decomposition of Nitrobenzene in Aqueous Solution by Ag/Cu₂O Assisted with Persulfate under Visible Light Irradiation. *Photochem* **2021**, *1*, 220–236. <https://doi.org/10.3390/photochem1020013>

Received: 15 July 2021

Accepted: 16 August 2021

Published: 27 August 2021

Publisher's Note: MDPI stays neutral with regard to jurisdictional claims in published maps and institutional affiliations.



Copyright: © 2021 by the authors. Licensee MDPI, Basel, Switzerland. This article is an open access article distributed under the terms and conditions of the Creative Commons Attribution (CC BY) license (<https://creativecommons.org/licenses/by/4.0/>).

1. Introduction

Nitrobenzene is commonly used for the manufacture of polyurethane by way of intermediates of aniline. It has been also applied in the following industries: plastics, pesticides, pharmaceuticals and explosives [1]. Due to high risks for mutagenicity and carcinogenicity suffered, effluent contaminated with nitrobenzene and related derivatives would cause strong damage to the aqueous circumstances [2,3]. Consequently, much effort has been focused on the development of economically and effectively treating manners for industrial wastewater.

Advanced oxidation processes have been extensively explored for the mineralization of nitrobenzene in wastewater due to its resistance to biodegradation resulted from the electron-withdrawing property of nitro groups [4]. Firstly, much research has been carried out on hydroxyl radical-based processes, such as Fenton's methods [5–7], Fenton-like manners [8–10], Fenton reagents with auxiliary ultrasound [11] and Fenton reagents coupled with fluidization flow patterns [12,13]. Secondly, as commercial titanium dioxide is under investigation, the significant enhancement of the nitrobenzene destruction efficiency took advantage of doping ferric oxides, which successfully prevent the combination of photon-induced electrons with holes [14]. In another aspect, ultraviolet absorbance band was obviously changed to the visible light range by virtue of impregnating ammonium and cerium nitrates simultaneously [15,16]. On the other hand, ozone supported with ultrasound was employed for nitrobenzene removal, wherein hydroxyl radicals were claimed to be predominant oxidizing agents [17,18]. The oxidation of nitrobenzene through the catalysis of ozone over aluminum silicate was performed to elucidate the influences of operating parameters [19,20]. Additionally, the electrochemical oxidation of nitrobenzene was

conducted by the modified PbO_2 electrode plates, which were incorporated with titanium dioxide nanotubes, resulting in ordered arrangement and surface areas extended [21,22].

To date, sulfate-radical-related processes have been also dedicated to decomposing nitrobenzene in wastewater. The thermal activation of persulfate was effective for the disposal of effluents contaminated with nitrobenzene, wherein reaction pathways consist of 2-nitrophenol, 4-nitrophenol, 2,6-dinitrophenol and 2,4-dinitrophenol [23]. Except ferrous ions for the catalytic transformation of persulfate to sulfate radicals, zinc metal and magnetized iron metal also exhibited fruitful performance on nitrobenzene removal [24–26]. With a view to promoting nitrobenzene abatement, experiments were carried out utilizing persulfate anions irradiated with ultraviolet light [27]. Even though persulfate activated with photoelectrons descended from semiconductors excited by visible light, this has been barely studied in regard to nitrobenzene oxidation. As expected, the band gap energy of semiconductors meets the luminous energy of the incident light, leading to the generation of photo-induced electron–hole pairs. Persulfate anions would be transformed into reactive sulfate radicals via the activation of photo-induced electrons [28].

In this research, an innovative technique for the effective removal of nitrobenzene in wastewater was developed. Considerable sulfate radicals could be produced by way of persulfate via photoelectrons originated from $\text{Ag}/\text{Cu}_2\text{O}$ irradiated with visible light, which are well known as semiconductors [29–32]. The influences of operating parameters on the nitrobenzene degradation behaviors were explored, such as persulfate concentrations and $\text{Ag}/\text{Cu}_2\text{O}$ dosages. Nitrobenzene decomposition pathways catalyzed by the $\text{Ag}/\text{Cu}_2\text{O}$ coupled with persulfate under visible light irradiation would be investigated in the meantime.

2. Experimental Methods

2.1. Testing of Photocatalytic Oxidation of Nitrobenzene by $\text{Ag}/\text{Cu}_2\text{O}$ with Assistance of Persulfate

The experimental system containing the main equipment was referred to in our previous report [33]. The photocatalytic cell was a quartz cylinder fitted internally with a magnetic stirrer and cooling coils, in which the testing temperature was maintained through a thermostat (PIIN JIA Technol. Co. New Taipei City, Taiwan). Visible light irradiation was supplied from twelve lamps (8.6 W each) surrounding the cell with three chief peaks of 438 nm, 550 nm and 619 nm, respectively (Philips Corp. PL-S, Hanover, MD, US). Owing to consistence with practical concentrations of industrial wastewater, feedstock was prepared at 1.0 mM concentrations of nitrobenzene ($\geq 99.5\%$, Riedel-de Haen, Seelze, Germany) [34], being well agitated with proper weights of sodium persulfate ($\geq 99.5\%$, Fluka, Seelze, Germany) beforehand. The $\text{Ag}/\text{Cu}_2\text{O}$, manufactured from Cu_2O powder (SHOWA, Tokyo, Japan) by incipient impregnation with 1–5 wt% of silver nitrate ($\geq 99.5\%$, Fluka), respectively, and sequential 3 h calcination at 473 K by sieving with 400 mesh [35], was carefully loaded into the basket and fixed near the center of photocatalytic cell. For the duration of tests, samples were taken from the cell at constant time intervals, and sequentially quenched to the temperature of 273 ± 0.5 K to terminate nitrobenzene oxidation [36]. Aqueous samples were executed on total organic carbon analyses to evaluate residual organic compounds. The $\text{Ag}/\text{Cu}_2\text{O}$ separated from oxidation tests were examined by an X-ray photoelectron spectrometer. In this work, experiments were performed in a series of persulfate concentrations of 35.0 to 70.0 mM to elucidate the sulfate radical effect at the pH values of 5 to 6. Photocatalytic tests under diverse dosages of $\text{Ag}/\text{Cu}_2\text{O}$ (1.05 up to 1.50 g L^{-1}) were carried out for enhancement on nitrobenzene removal efficiency. All experiments were undertaken repeatedly for the affirmation of data reliability.

2.2. Total Organic Carbon (TOC) Analysis

Within the duration of photocatalytic testing by $\text{Ag}/\text{Cu}_2\text{O}$ assisted with persulfate, wastewater was periodically sampled and measured, utilizing a TOC analyzer (GE Corp. Sievers InnovOx, Boston, MA, USA). The hydrocarbons involved were completely oxidized into carbon dioxide and quantified through nondispersive infrared (NDIR) analyses,

wherein persulfate mineralization was carried out under supercritical water conditions. On the contrary, non-hydrocarbons were exhausted in the species of carbonic acid. In this work, the TOC concentrations reported were calibrated to the standard curve, fulfilled faithfully in the range (0–5.0 mM) utilizing standard chemicals of potassium hydrogen phthalate.

2.3. Physicochemical Properties of Ag/Cu₂O

The crystal compositions of fresh Ag/Cu₂O semiconductors were examined using an X-ray diffractometer (Rigaku, MiniFlex II, Tokyo, Japan) integrated with high-intensity monochromated CuK α radiation at the wavelength of 0.15418 nm, operating with the current of 30 mA and 40 kV volts over the 2 θ range from 10 to 80 degrees. For the inspection of surface morphology and silver content impregnated on Ag/Cu₂O semiconductors, surface scanning was executed by a field-emission scanning electron microscope (JEOL, JSM-6500F) equipped with an energy dispersive X-ray spectroscope (JEOL, JED-2300). As far as light absorption band is concerned, the Ultraviolet–Visible diffuse reflectance spectra on Ag/Cu₂O were measured using a UV–Vis spectrometer (PerkinElmer, Lambda-850, Waltham, MA, USA), of which wavelength was among the range of 250 to 800 nm with reference to BaSO₄. The photocurrent measurements of the samples were carried out using a potentiostat (Zensor, ECAS-100, Etterbeek, Belgium) under continuous visible light irradiation (Philips, PL-S), wherein a Pt wire served as an auxiliary electrode, coated with Ag/Cu₂O and polymer electrolyte membrane, and was referenced to a saturated calomel electrode. Further, electronic states of fresh and reacted Ag/Cu₂O semiconductors were monitored by means of XPS spectra from an X-ray photoelectron spectrometer (Kratos Analytical Ltd. Axis Ultra, Manchester, UK), in which monochromated AlK α irradiation was used as a light source and the binding energy of samples was calibrated to 284.8 eV for C 1s core level of adventitious carbon.

2.4. Gas Chromatography–Mass Spectrometry (GC-MS) Analysis

A proper amount of wastewater was withdrawn from the photocatalytic cell after nitrobenzene oxidation testing for 30 min. The microextraction fiber spread with carboxen/polydimethylsiloxane (Supelco, Bellefonte, PA, USA) was added into aqueous solution for the effective adsorption of degradation intermediates. Then, the fiber was directly packed into a micro-needle which was immediately injected into the orifice of the gas chromatograph–mass spectrometer (Hewlett Packard, MASS 59864B/5973, Palo Alto, CA, USA). The metal capillary column for ingredient separation was used at the dimension of 30 m \times 0.25 mm (Ultra ALLOY UA-5), wherein helium gas served as the carrier gas. The degradation intermediates resolved were trustworthy based on mass spectra obtained in comparison with those of standards.

2.5. Scavenging Effects

In order to disclose the main oxidants on the mineralization of nitrobenzene, testing was conducted in the presence of diverse scavengers simultaneously, such as methanol, 1-propanol and benzene, respectively [37,38]. The nitrobenzene degradation percentage was determined on the basis of the peak area (262 nm) shown in a UV–Vis spectrophotometer (PerkinElmer, Lambda 850) [8]. In the course of pretesting, benzene was verified as the most sharp scavenger. The benzene scavenging effect may represent sulfate radical yields at different experimental conditions. To evaluate sulfate radical yields, the decrement of nitrobenzene degradation percentage was examined upon the addition of suitable amounts of benzene scavenger into wastewater.

3. Results and Discussion

3.1. Comparison of Photocatalytic Oxidation by Ag/Cu₂O Alone and Ag/Cu₂O Assisted with Persulfate Respectively

Figure 1 demonstrates the time flow patterns of TOC removal efficiency executed by photocatalytic oxidation over Ag/Cu₂O alone and Ag/Cu₂O aided with persulfate,

respectively. Apparently, the nitrobenzene removal rate caused by Ag/Cu₂O supported with persulfate process was much higher than those simply using persulfate anions, Cu₂O and Ag/Cu₂O alone. Noteworthily, Ag(1%)/Cu₂O integrated with persulfate displayed a synergistic performance in comparison with photocatalytic behaviors exhibited with the Ag(1%)/Cu₂O and persulfate individually. The observation could be ascribed to great enhancement on reactive sulfate radical yields. In fact, persulfate anions have been successfully transformed to sulfate radicals through the photocatalysis of Cu₂O [39]. It has been also recognized that Ag metal functions as an electron sink and strengthens charge separation, leading to the repression of the combination of photo-induced electrons and holes over Cu₂O [40,41]. As expected, a higher extent of Ag metal doped on the surface of Cu₂O gave rise to higher nitrobenzene removal efficiency (refer to Figure 2). The main reactions that occurred could be concluded as follows.

- (1) $\text{Ag/Cu}_2\text{O} + h\nu \rightarrow h^+_{\text{vb}} + e^-_{\text{cb}}$
- (2) $\text{S}_2\text{O}_8^{2-} + e^-_{\text{cb}} \rightarrow \text{SO}_4^{\bullet-} + \text{SO}_4^{2-}$
- (3) $\text{SO}_4^{2-} + h^+_{\text{vb}} \rightarrow \text{SO}_4^{\bullet-}$
- (4) $\text{H}_2\text{O} + h^+_{\text{vb}} \rightarrow \text{HO}\bullet + \text{H}^+$

where e^-_{cb} represents photo-induced electrons in the conduction band and h^+_{vb} represents photo-induced holes in the valence band. Ag(5%)/Cu₂O was chosen as a candidate for next testing due to its better nitrobenzene degradation behavior.

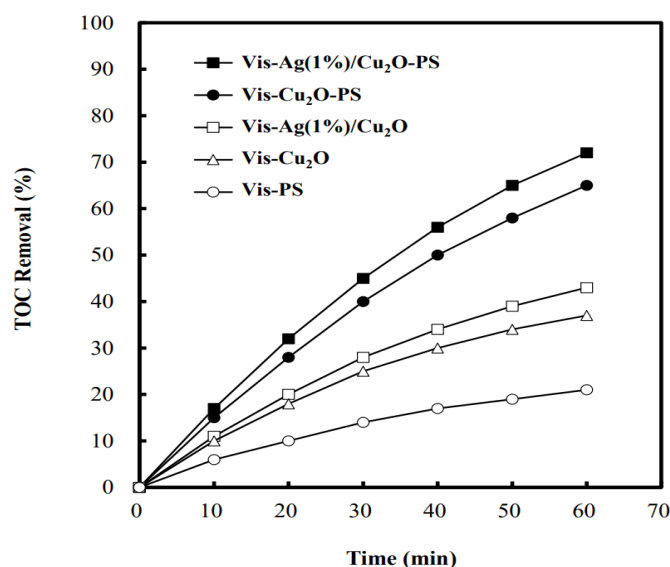


Figure 1. Time flow patterns of TOC removal efficiency by Cu₂O, persulfate, Ag(1 wt%)/Cu₂O, Cu₂O-persulfate and Ag(1 wt%)/Cu₂O-persulfate, respectively under the conditions of visible light power = 103.2 W, persulfate concentration = 50 mM, Cu₂O or Ag(1 wt%)/Cu₂O dosage = 1.20 g L⁻¹ and T = 318 K.

XPS measurements were carried out to elucidate surface electronic states of Ag(5%)/Cu₂O. Figure 3 illustrates the Cu2p XPS spectra of fresh Ag(5%)/Cu₂O and reacted Ag(5%)/Cu₂O. As far as fresh Ag(5%)/Cu₂O semiconductor is concerned, two peaks centered at 933.0 and 952.0 eV were clearly found, which were appointed to the binding energy of Cu⁺2p_(3/2) and Cu⁺2p_(1/2), respectively [42–44]. With regard to reacted Ag(5%)/Cu₂O, four peaks centered at 933.5, 941.0, 953.0 and 961.0 eV were present, which were separately assigned to the binding energy of Cu⁺2p_(3/2), Cu²⁺2p_(3/2), Cu⁺2p_(1/2) and Cu²⁺2p_(1/2) [45,46]. Obviously, Cu⁺ cations on the surface of reacted Ag(5%)/Cu₂O shifted to higher oxidation states in comparison with the fresh one, in consideration of the migration of photo-induced electrons to persulfate anions [39,47]. The observations manifest the above hypothesis that persulfate anions could be converted into sulfate radicals upon activation by photo-induced electrons. Instead, sulfate anions may be also

transformed to sulfate radicals via photo-induced holes over Ag(5%)/Cu₂O [48]. It makes partial contributions for nitrobenzene oxidation.

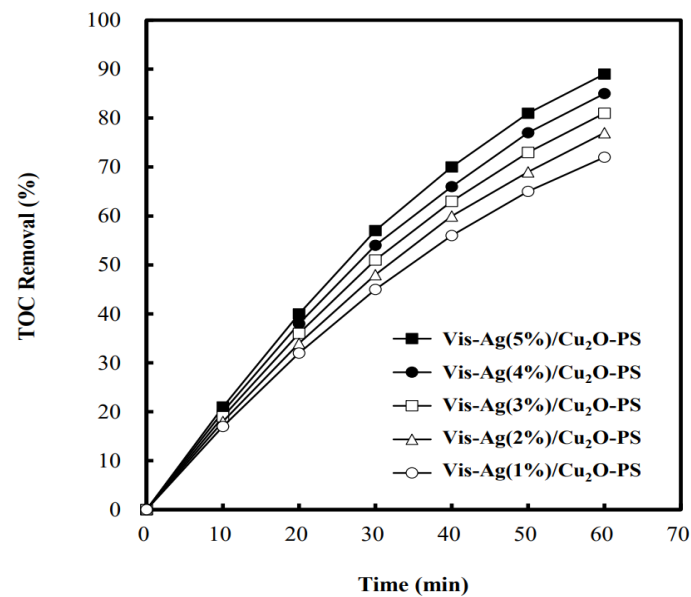


Figure 2. Effect of silver metal contents on the TOC removal efficiency under the conditions of visible light power = 103.2 W, persulfate concentration = 50 mM, Ag/Cu₂O dosage = 1.20 g L⁻¹ and T = 318 K.

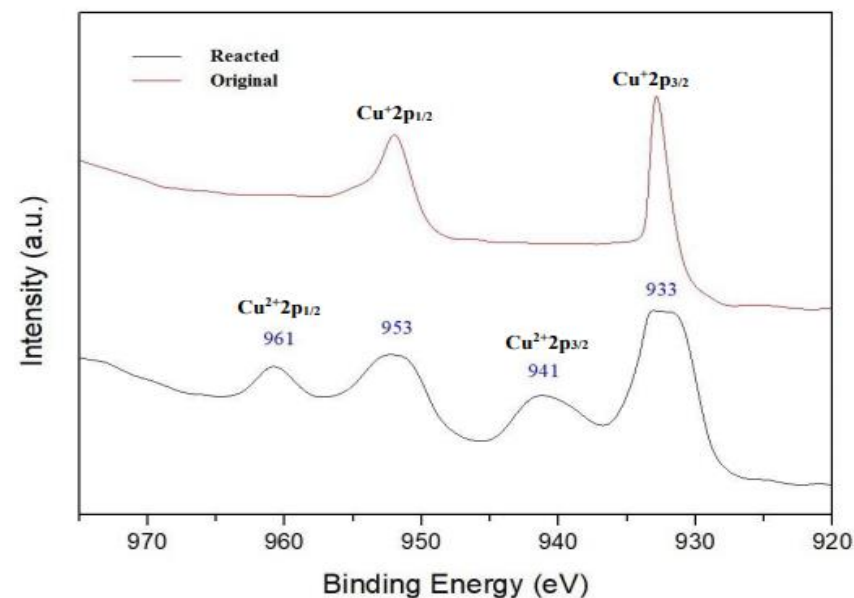


Figure 3. X-ray photoelectron spectra of Cu⁺2p or Cu²⁺2p core level for original Ag(5 wt%)/Cu₂O and reacted Ag(5 wt%)/Cu₂O semiconductors.

3.2. Physicochemical Properties of Ag/Cu₂O

The X-ray diffraction patterns of Ag/Cu₂O semiconductors are displayed in Figure 4. Major peaks in the spectra were matched with crystal planes of Cu₂O, wherein the characteristic peak at 2θ value of 36.5° was ascribed to the (111) plane [48,49]. Conversely, the diffraction peak at 2θ values of 38.1° was appointed to the (111) plane of Ag metal [50]. It is evident that slight weight of Ag metal was doped on the surface of Cu₂O. Figure 5 presents field-emission SEM images of Ag/Cu₂O semiconductors. Obviously, the majority of the Cu₂O surface was smooth. In contrast, a few irregular-shaped sediments were found over

Ag/Cu₂O and more clumps of particles were observed upon increasing Ag extent. It is apparent that Ag metal was well spread on the surface of Cu₂O. The Energy-Dispersive X-ray Mapping analysis on Ag/Cu₂O is illustrated in Figure 6. Ag metal was well dispersed, and its contents measured agreed with those impregnated theoretically (see Table 1).

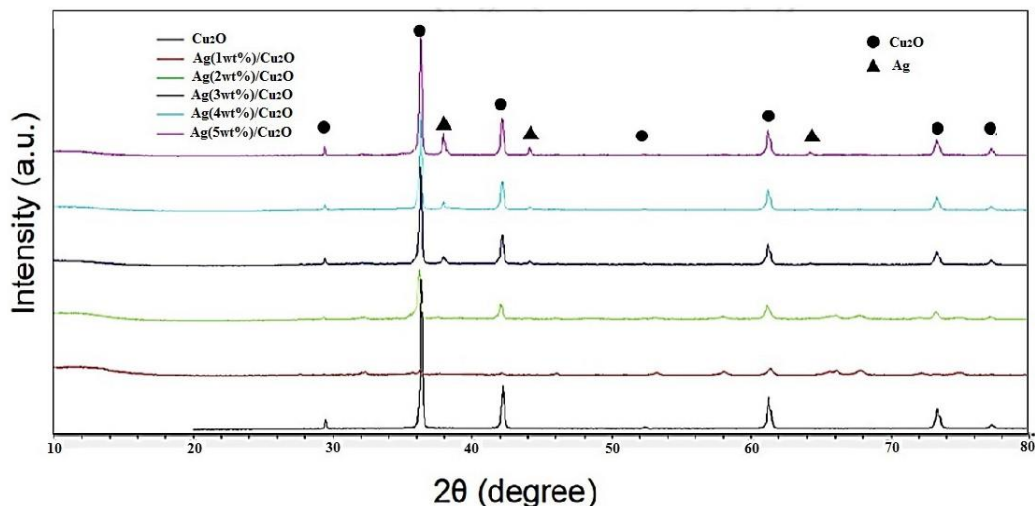


Figure 4. The XRD patterns of Cu₂O and Ag/Cu₂O semiconductors.

Figure 7 depicts the UV–Vis diffuse reflectance spectra for a series of Ag/Cu₂O semiconductors. The analogous spectra were observed between Ag/Cu₂O and Cu₂O at the absorbance wavelength between 400 and 530 nm, which fall into the visible light range. Particularly, the light absorbance intensity of Ag/Cu₂O was stronger than that of Cu₂O. It implies that Ag/Cu₂O semiconductors are more responsive to the visible light irradiation. This phenomenon could be mainly ascribed to Ag metal dopant, creating an electron sink and restraining a combination of photo-induced electrons with holes over Cu₂O [51,52]. Further, the Ag/Cu₂O band gap energy was resolved by means of a Tauc's equation $[(\alpha h\nu)^{1/n} = A(h\nu - E_g)]$, in which $h\nu$ stands for incident optical energy. The “n” parameter was set at the value of 1/2 according to the electronic transition state of Ag/Cu₂O semiconductors. The draft of $(\alpha h\nu)^2$ varied with incident optical energy; $(h\nu)$ was drawn to obtain the band gap energy by intercepting tangent lines to the X-axis [53–55]. Consequently, the Cu₂O band gap energy was determined to be 2.17 eV, consistent with that reported by Muthukumaran et al. [56]. For a series of Ag/Cu₂O semiconductors, the band gap energy was estimated to be 2.06, 1.92, 1.75, 1.55 and 1.43 eV, respectively, upon increasing Ag metal doping (refer to Table 2). The superior photocatalytic performance presented by Ag(5%)/Cu₂O could be reasonably attributed to a significant yield of photo-induced electrons, caused by a lower band gap energy. In other words, the optical energy of visible light could stimulate Ag/Cu₂O semiconductors for the generation of electron–hole pairs. Persulfate anions would be effectively converted into reactive sulfate radicals via activation of photo-induced electrons. Likewise, photo-induced holes may also transform sulfate anions into sulfate radicals. Figure 8 illustrates transient photocurrent of Cu₂O and Ag(5%)/Cu₂O excited under visible light irradiation. The photocurrent intensity of the latter was clearly higher than that of the former. It means that Ag(5%)/Cu₂O possessed the higher yield of photo-induced electron [40,41]. The results support the issue of the inhibition of a combination of photo-induced electrons and holes over Cu₂O through the impregnation of Ag metal.

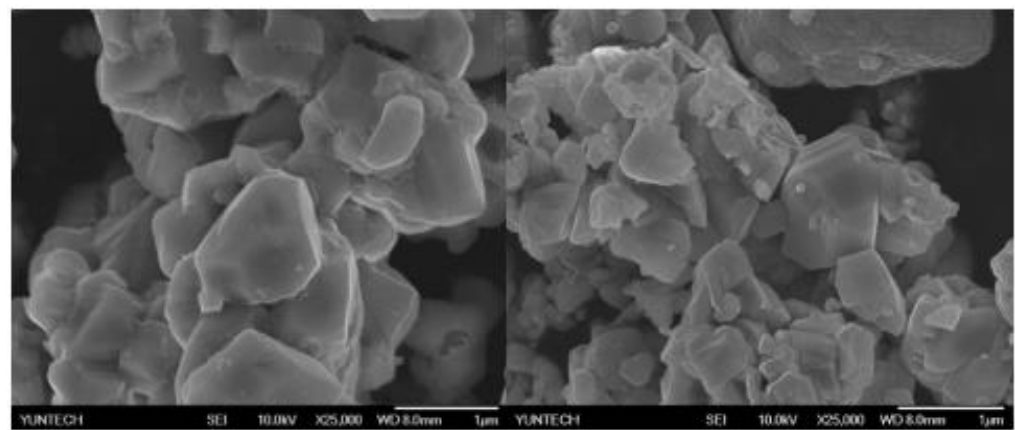
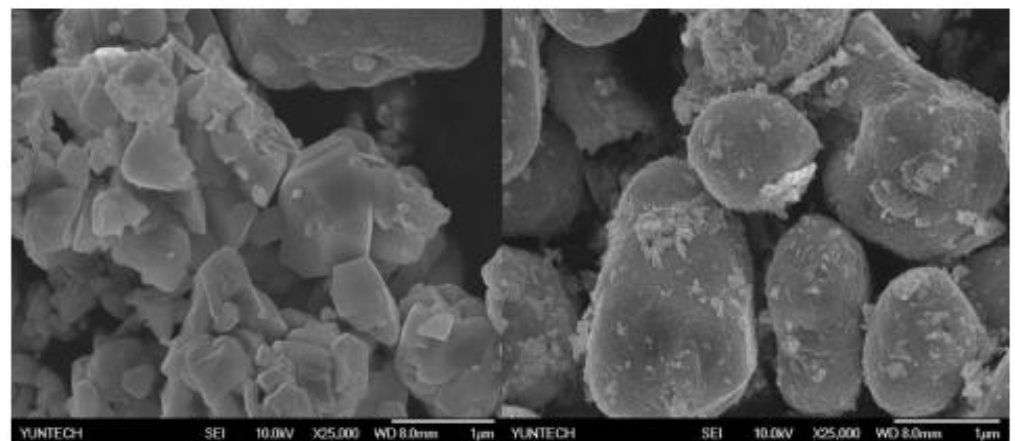
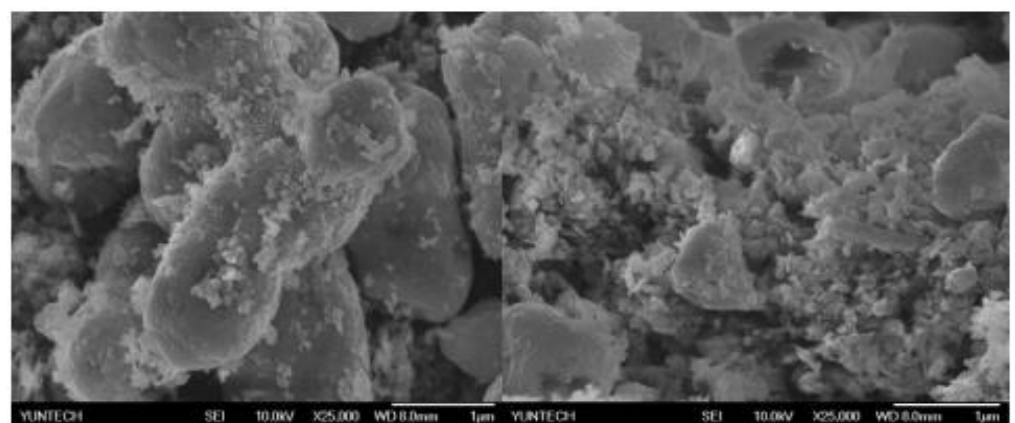
(a) Cu₂O(b) Ag(1wt%)/Cu₂O(c) Ag(2wt%)/Cu₂O(d) Ag(3wt%)/Cu₂O(e) Ag(4wt%)/Cu₂O(f) Ag(5wt%)/Cu₂O

Figure 5. FE-SEM images of the (a) Cu₂O, (b) Ag(1 wt%)/Cu₂O, (c) Ag(2 wt%)/Cu₂O, (d) Ag(3 wt%)/Cu₂O, (e) Ag(4 wt%)/Cu₂O and (f) Ag(5 wt%)/Cu₂O semiconductors.

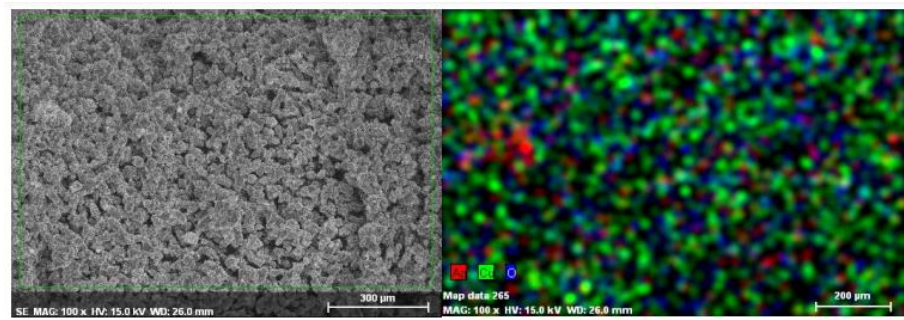
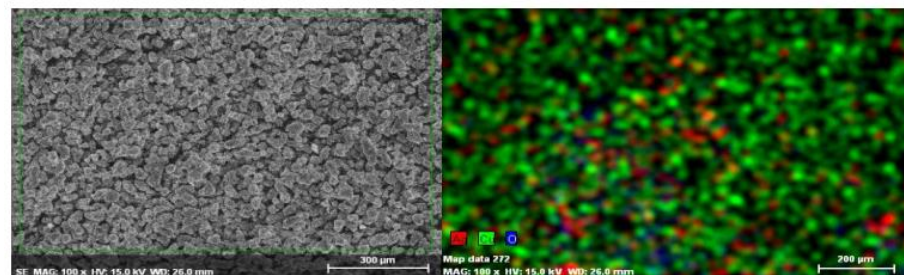
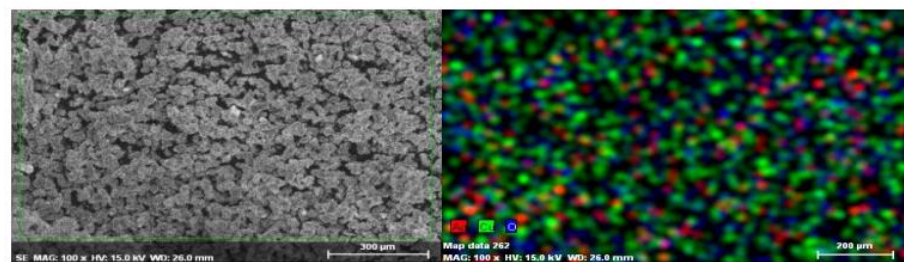
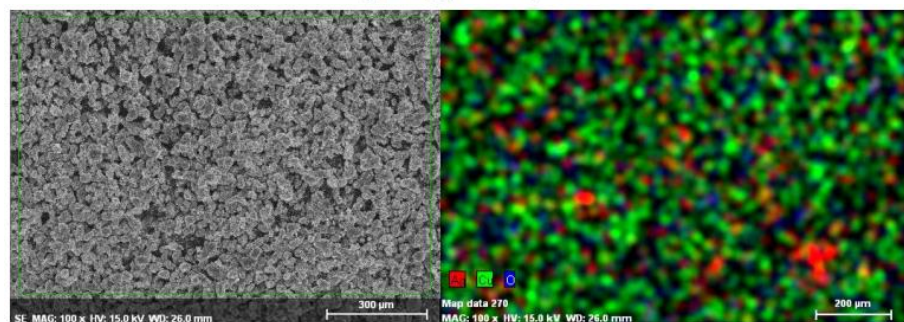
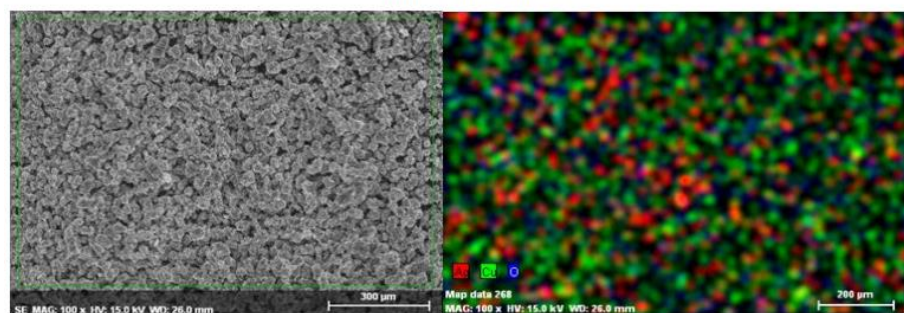
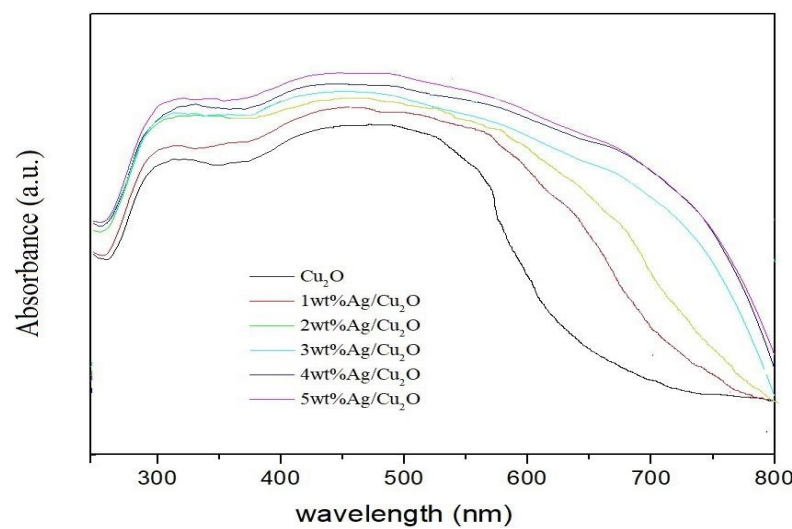
(a) Ag(1wt%)/Cu₂O(b) Ag(2wt%)/Cu₂O(c) Ag(3wt%)/Cu₂O(d) Ag(4wt%)/Cu₂O(e) Ag(5wt%)/Cu₂O

Figure 6. The EDS Mapping analyses on Ag/Cu₂O semiconductors: (a) Ag(1 wt%)/Cu₂O, (b) Ag(2 wt%)/Cu₂O, (c) Ag(3 wt%)/Cu₂O, (d) Ag(4 wt%)/Cu₂O and (e) Ag(5 wt%)/Cu₂O.

Table 1. The elemental compositions of semiconductors by EDS analyses.

Semiconductor	Ag(wt%)	Cu(wt%)	O(wt%)
Cu ₂ O	0.00	85.81	14.19
Ag(1 wt%)/Cu ₂ O	1.15	87.41	11.44
Ag(2 wt%)/Cu ₂ O	2.05	87.56	10.39
Ag(3 wt%)/Cu ₂ O	3.56	84.32	12.12
Ag(4 wt%)/Cu ₂ O	4.99	82.39	12.62
Ag(5 wt%)/Cu ₂ O	6.84	80.67	12.49

**Figure 7.** UV-Vis diffuse reflectance spectra of Cu₂O, Ag(1 wt%)/Cu₂O, Ag(2 wt%)/Cu₂O, Ag(3 wt%)/Cu₂O, Ag(4 wt%)/Cu₂O and Ag(5 wt%)/Cu₂O semiconductors.**Table 2.** The band gap energy of semiconductors by UV-Vis DRS analyses.

Semiconductor	Band Gap Energy (eV)
Cu ₂ O	2.17
Ag(1 wt%)/Cu ₂ O	2.06
Ag(2 wt%)/Cu ₂ O	1.92
Ag(3 wt%)/Cu ₂ O	1.75
Ag(4 wt%)/Cu ₂ O	1.55
Ag(5 wt%)/Cu ₂ O	1.43

3.3. Effect of Scavenger Dosages on Photocatalytic Oxidation by Ag/Cu₂O Assisted with Persulfate

Equivalent concentrations of benzene, 1-propanol and methanol were individually blended with nitrobenzene in wastewater to disclose reactive radicals under photocatalysis by Ag/Cu₂O with assistance of persulfate. As demonstrated in Figure 9, nitrobenzene removal efficiency was sharply faded upon the addition of benzene, due to a high reaction rate constant for benzene and sulfate radicals ($3 \times 10^9 \text{ M}^{-1} \text{ s}^{-1}$) [37]. Alternatively, 1-propanol and methanol slightly suppressed the nitrobenzene removal rate, on account of moderate rate constants for 1-propanol and methanol, with sulfate radicals being $6.0 \times 10^7 \text{ M}^{-1} \text{ s}^{-1}$ and $3.2 \times 10^6 \text{ M}^{-1} \text{ s}^{-1}$, respectively [57]. It deserves noting that the extent of nitrobenzene removal percentages faded corresponds to the reactive activity for various scavengers and sulfate radicals. It was revealed that sulfate radicals were principal oxidants for nitrobenzene degradation in wastewater.

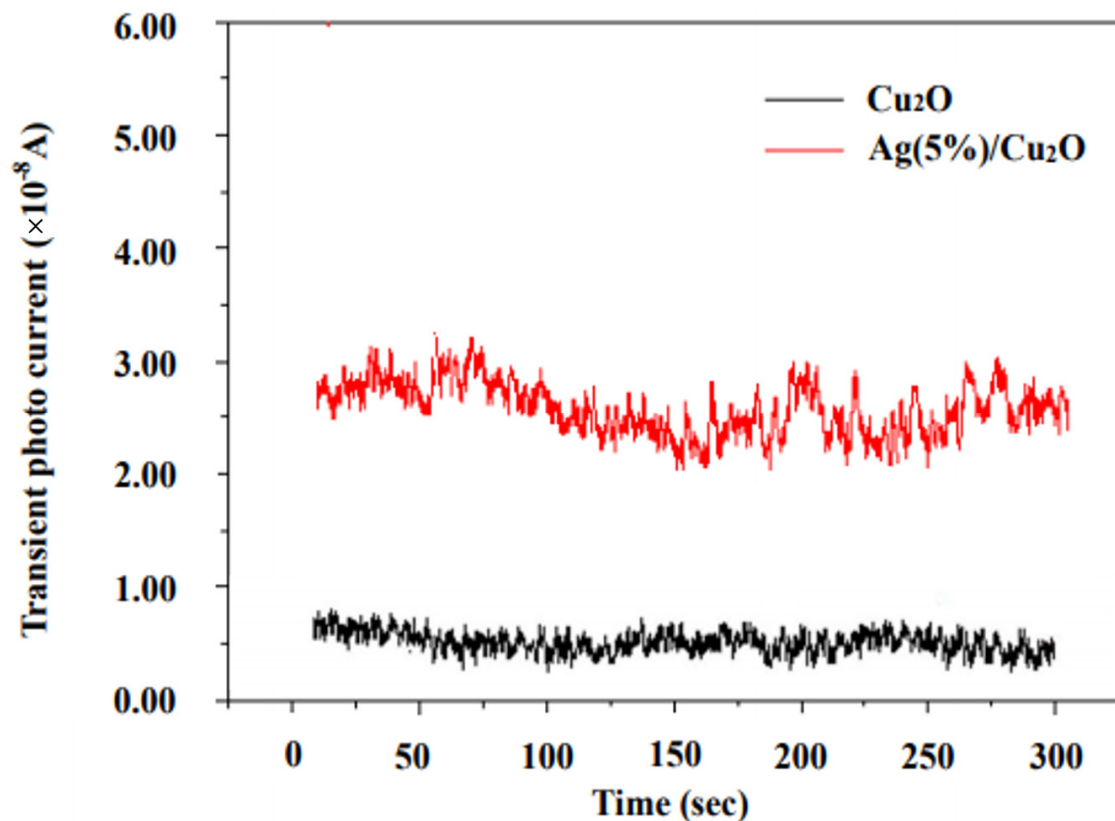


Figure 8. The transient photocurrent analyses of Cu_2O and $\text{Ag}(5\%)/\text{Cu}_2\text{O}$ under visible light irradiation.

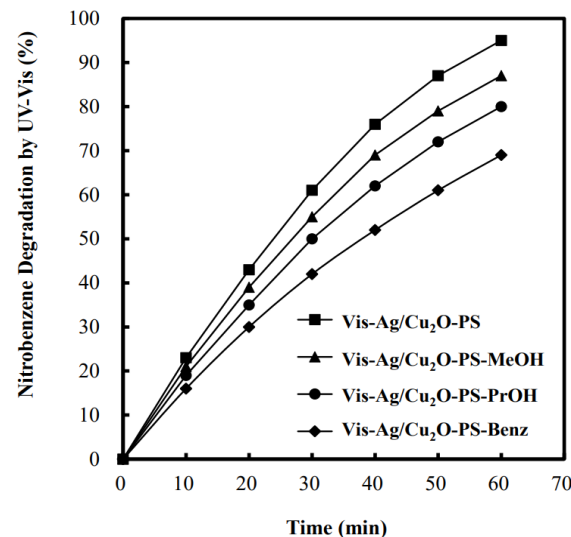


Figure 9. Effect of coexistence of benzene, 1-propanol and methanol, respectively, on the nitrobenzene degradation efficiency.

3.4. Effect of Persulfate Concentrations on Photocatalytic Oxidation by $\text{Ag}/\text{Cu}_2\text{O}$ Assisted with Persulfate

The optimal persulfate concentration for nitrobenzene elimination should be determined in consideration of commercialization. As presented in Figure 10a, the time flow patterns of TOC removal efficiency were dependent on persulfate concentrations. Undoubtedly, increasing persulfate concentrations enhanced nitrobenzene removal rates, wherein high sulfate radical yields could be sensibly expected. Nonetheless, the nitrobenzene removal efficiency faded under an excess persulfate concentration (70 mM). This phenomenon

may be interpreted with probable side reactions for the overdosage of persulfate anions and sulfate radicals [38,58]. Further, the photocatalytic oxidation of nitrobenzene was performed in the existence of benzene scavengers to discriminate sulfate radical yields under various persulfate concentrations (refer to Figure 10b). Definitely, the scavenging effect dramatically displays an analogy between sulfate radical yields and TOC removal efficiency. Accordingly, sulfate radicals were likely to be responsible for nitrobenzene oxidation.

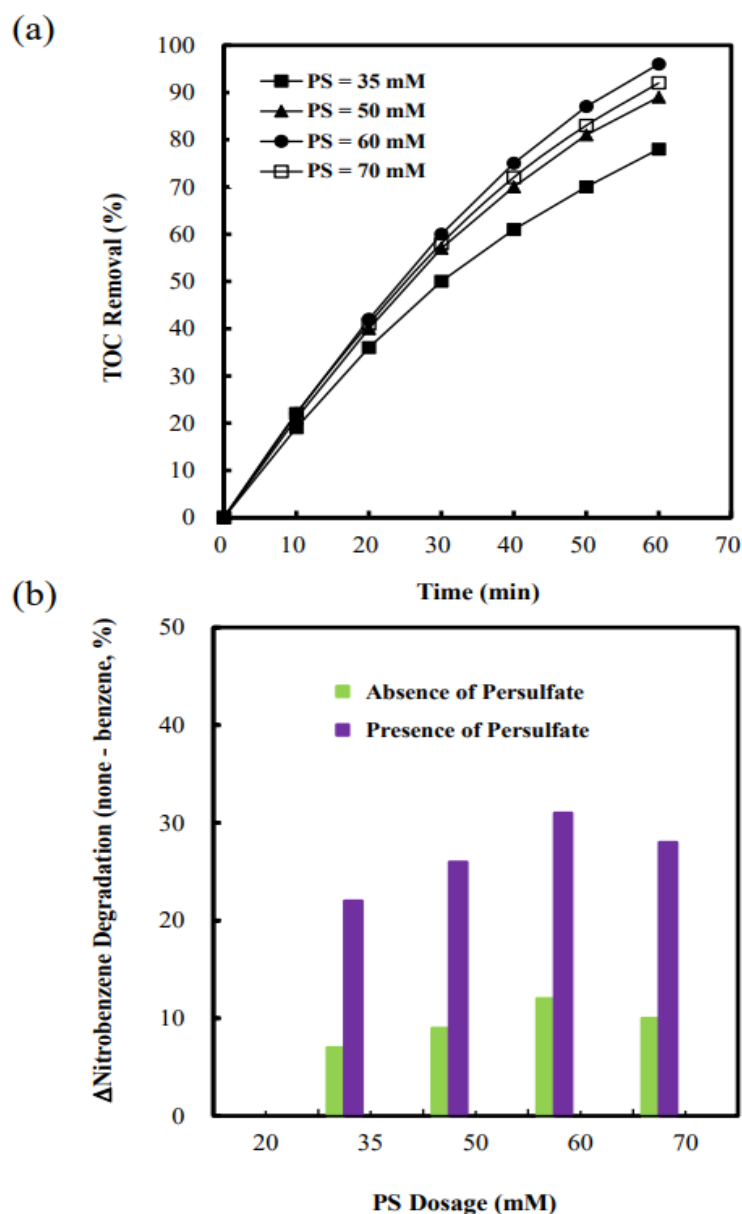


Figure 10. (a) Effect of persulfate concentrations on the TOC removal efficiency under the conditions of visible light power = 103.2 W, Ag(5 wt%)/Cu₂O dosage = 1.20 g L⁻¹ and T = 318 K. (b) The difference of nitrobenzene degradation efficiency between the absence of benzene and presence of benzene monitored by UV-Vis and served as scavenging effect under the conditions of visible light power = 103.2 W, Ag(5 wt%)/Cu₂O dosage = 1.20 g L⁻¹ and T = 318 K.

3.5. Effect of Ag/Cu₂O Dosage on Photocatalytic Oxidation by Ag/Cu₂O Assisted with Persulfate

An optimal dosage of Ag/Cu₂O semiconductor needs to be essentially established from the process design viewpoint. Figure 11a illustrates the time flow patterns of TOC removal efficiency as functions of Ag/Cu₂O dosages. Evidently, the nitrobenzene degradation rate raised with an increment of Ag/Cu₂O dosages, whereas it reduced under

overdosages of Ag/Cu₂O ($\geq 1.50 \text{ g L}^{-1}$). The improvement in the nitrobenzene removal efficiency could be attributed to high sulfate radical yields, caused by the massive activation of persulfate anions via the photocatalysis of Ag/Cu₂O. Conversely, lesser semiconductors received optical energy because of scatter of visible light irradiation, resulting from excessive dosages of Ag/Cu₂O powder [59]. Nitrobenzene decomposition efficiency likewise displayed a similar trend as benzene scavenging behaviors (refer to Figure 11b). The outcomes convince us that sulfate radicals were chief oxidants toward nitrobenzene destruction. Especially, the optimal conditions for complete mineralization of nitrobenzene were determined as follows: visible light power = 103.2 W, persulfate concentration = 60 mM, Ag/Cu₂O dosage = 1.35 g L⁻¹ and T = 318 K. In this work, the photocatalytic stability of Ag/Cu₂O was proved via repetitions of five tests (shown in Figure 12). Evidently, nitrobenzene removal efficiency reached almost 98% during the overall experiment. That convinces us of the feasibility for the potential application of Ag/Cu₂O to industrial wastewater treatment.

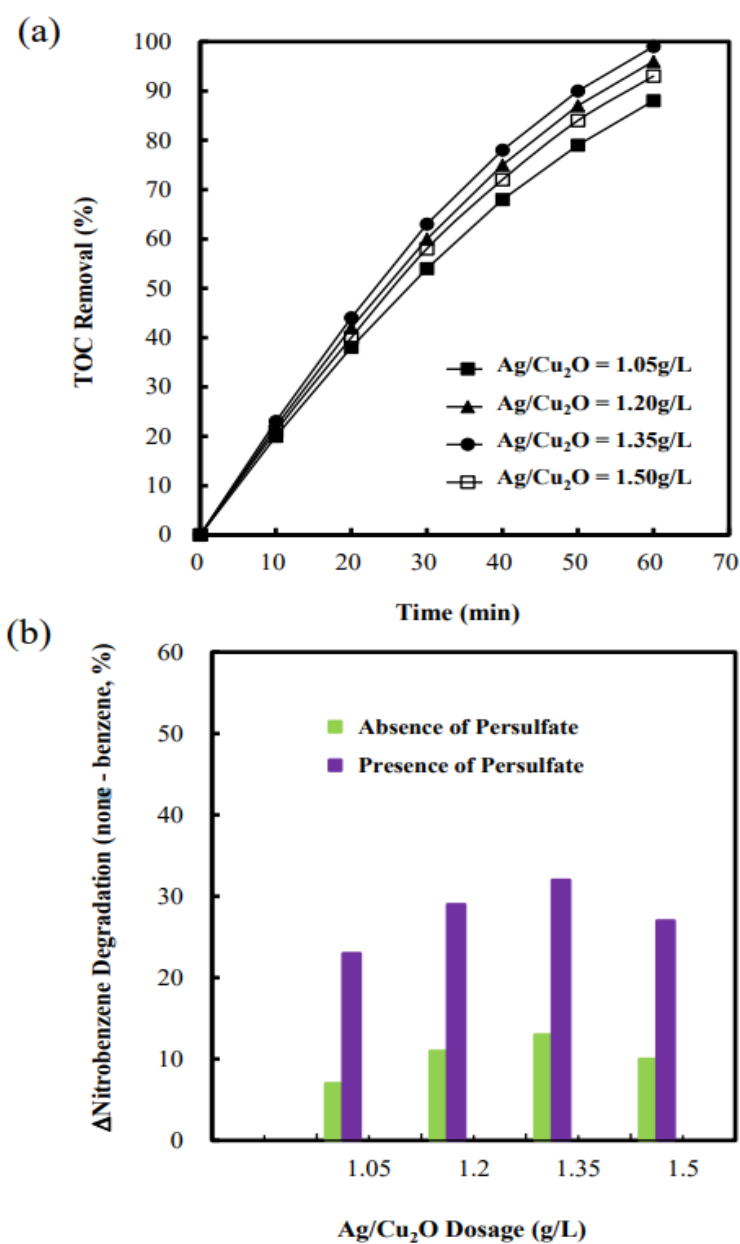


Figure 11. (a) Effect of Ag(5 wt%)/Cu₂O dosages on the TOC removal efficiency under the conditions of visible light power = 103.2 W, persulfate concentration = 60 mM and T = 318 K. (b) The difference

of nitrobenzene degradation efficiency between the absence of benzene and presence of benzene monitored by UV-Vis and served as scavenging effect under the conditions of visible light power = 103.2 W, persulfate concentration = 60 mM and T = 318 K.

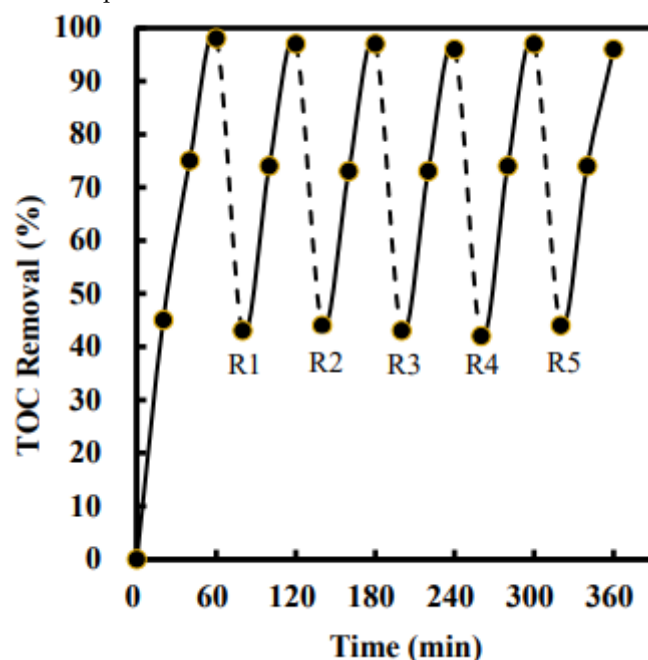


Figure 12. The photocatalytic stability of Ag(5 wt%)/Cu₂O examined by means of repetitions of five tests.

3.6. Reaction Pathways of Photocatalytic Oxidation of Nitrobenzene by Ag/Cu₂O Assisted with Persulfate

All reaction intermediates extracted from photocatalytic oxidation of nitrobenzene using Ag/Cu₂O with assistance of persulfate were examined by a GC-MS spectrometer. Table 3 summarizes the ingredients procured, including nitrobenzene used for raw materials, phenol, 2-nitrophenol, 3-nitrophenol, 4-nitrophenol, hydroquinone and *p*-benzoquinone. In consideration of the source of 2-nitrophenol, 3-nitrophenol and 4-nitrophenol, it was believed that nitrobenzene underwent O₂ addition, followed with HO₂• elimination for the generation of hydroxycyclohexadienyl radicals and sequential hydroxylated compounds [57,60]. Phenol was clearly monitored as an intermediate because of the probable occurrence of nitrophenol denitration [61]. Afterward, phenol ordinarily executed oxidation reaction to hydroquinone, accompanied with successive hydrogen abstraction to *p*-benzoquinone. Ultimately, nitrobenzene would be mineralized into nitrate ions (analyzed by UV-Vis 313 nm), water and carbon dioxide. Based on most degradation intermediates cautiously identified, the hypothesized pathways for photocatalytic oxidation of nitrobenzene by Ag/Cu₂O aided with persulfate is demonstrated in Figure 13.

Table 3. Compositions of nitrobenzene and reaction intermediates identified by GC-MS.

Component	m/z (Relative Abundance, %)
Feedstock	
Nitrobenzene	50 (15.7), 51 (37.7), 65 (13.6), 74 (9.0), 77 (100), 78 (7.5), 93 (16.9), 123(70.2)
Reaction intermediate	
Phenol	38 (5.4), 39 (12.5), 40 (6.9), 55(6.4), 63 (6.5), 65 (21.0), 66 (27.4), 94 (100), 95 (7.7)
2-Nitrophenol	39 (15.7), 53 (9.8), 63 (20.2), 64 (13.9), 65 (25.5), 81 (19.6), 109 (18.2), 139 (100)
3-Nitrophenol	39 (35.9), 53 (10.7), 63 (14.7), 64 (7.9), 65 (63.7), 81 (15.8), 93 (51.4), 139 (100)
4-Nitrophenol	39 (44.2), 53 (23.3), 63 (28.1), 65 (79.9), 81 (33.0), 93 (26.9), 109 (67.1), 139 (100)
Hydroquinone	39 (6.9), 53 (14.4), 54 (12.9), 55 (10.5), 81 (25.3), 82 (12.3), 110 (100), 143 (9.6)
<i>p</i> -Benzoquinone	26 (18.1), 52 (17.9), 53 (17.1), 54 (63.3), 80 (28.2), 82 (36.3), 108 (100), 110 (12.1)

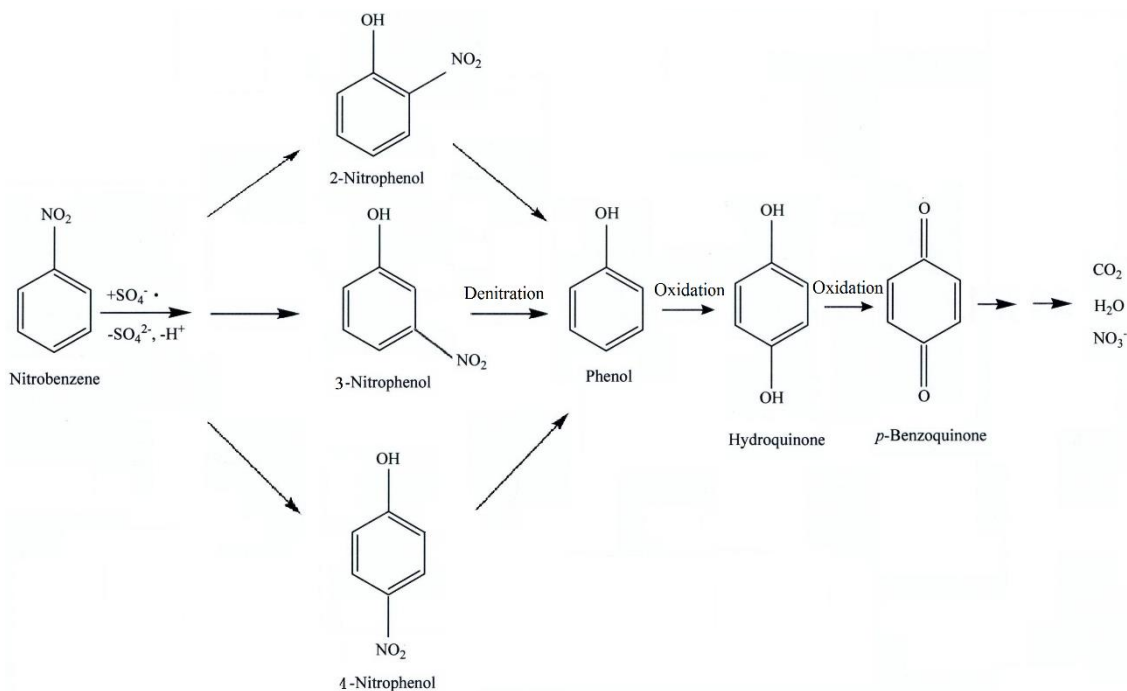


Figure 13. Overall reaction pathways of nitrobenzene in wastewater by photocatalysis of Ag/Cu₂O with assistance of persulfate.

4. Conclusions

In light of the above discussions, nitrobenzene contaminants were principally mineralized via reactive sulfate radicals, induced from persulfate anions activated effectively by the photocatalysis of Ag/Cu₂O semiconductors. It was intensely supported by benzene scavenger, wherein sulfate radical yields display an analogy with nitrobenzene removal efficiency. As far as GC-MS analyses are concerned, the overall reaction pathways on nitrobenzene oxidation could be proposed as follows. Firstly, nitrobenzene was transformed into hydroxycyclohexadienyl radicals, followed with oxidation step into 2-nitrophenol, 3-nitrophenol and 4-nitrophenol separately. Sequentially, nitrophenol-related compounds executed the denitration procedure to phenol, which was oxidized further for the synthesis of hydroquinone and *p*-benzoquinone. As expected, nitrobenzene would be nearly mineralized into carbon dioxide, nitrate ions and water. The striking results persuade us that the photocatalysis of Ag/Cu₂O coupled with persulfate is an effective and synergistic manner for disposal of industrial effluents.

Author Contributions: Conceptualization, W.-S.C. and J.-Y.C.; methodology, J.-Y.C.; software, J.-Y.C.; validation, W.-S.C., J.-Y.C.; formal analysis, J.-Y.C.; investigation, W.-S.C.; resources, W.-S.C.; data curation, J.-Y.C.; writing—original draft preparation, W.-S.C.; writing—review and editing, W.-S.C.; visualization, J.-Y.C.; supervision, W.-S.C.; project administration, W.-S.C.; funding acquisition, W.-S.C. All authors have read and agreed to the published version of the manuscript.

Funding: This research received no external funding.

Institutional Review Board Statement: Not applicable.

Informed Consent Statement: Not applicable.

Data Availability Statement: The study did not contain any data reported.

Conflicts of Interest: The authors declare no conflict of interest.

References

1. Weissermel, K.; Arpe, H.-J. *Ullmann's Encyclopedia of Industrial Chemistry*, 5th ed.; VCH: Weinheim, Germany, 1991; Volume A17.
2. Holder, J.W. Nitrobenzene carcinogenicity in animals and human hazard evaluation. *Toxicol. Ind. Health* **1999**, *15*, 445–457.
3. Wang, G.X.; Zhang, X.Y.; Yao, C.Z.; Tian, M.Z. Acute toxicity and mutagenesis of three metabolites mixture of nitrobenzene in mice. *Toxicol. Ind. Health* **2011**, *27*, 167–171. [[CrossRef](#)]
4. Zhu, L.; Ma, B.; Zhang, L. The study of distribution and fate of nitrobenzene in a water/sediment microcosm. *Chemosphere* **2007**, *69*, 1579–1585. [[CrossRef](#)]
5. Carlos, L.; Nichela, D.; Triszcz, J.M.; Felice, J.I.; Einschlag, F.S.G. Nitration of nitrobenzene in Fenton's processes. *Chemosphere* **2010**, *80*, 340–345. [[CrossRef](#)] [[PubMed](#)]
6. Jiang, B.C.; Lu, Z.Y.; Liu, F.Q.; Li, A.M.; Dai, J.J.; Xu, L.; Chu, L.M. Inhibiting 1,3-dinitrobenzene formation in Fenton oxidation of nitrobenzene through a controllable reductive pretreatment with zero-valent iron. *Chem. Eng. J.* **2011**, *174*, 258–265. [[CrossRef](#)]
7. Zhang, Y.; Zhang, K.; Dai, C.; Zhou, X.; Si, H. An enhanced Fenton reaction catalyzed by natural heterogeneous pyrite for nitrobenzene degradation in an aqueous solution. *Chem. Eng. J.* **2014**, *244*, 438–445. [[CrossRef](#)]
8. Nichela, D.A.; Berkovic, A.M.; Costante, M.R.; Juliarena, M.P.; Einschlag, F.S.G. Nitrobenzene degradation in Fenton-like systems using Cu(II) as catalyst. Comparison between Cu(II)- and Fe(III)-based systems. *Chem. Eng. J.* **2013**, *228*, 1148–1157. [[CrossRef](#)]
9. Duan, H.; Liu, Y.; Yin, X.; Bai, J.; Qi, J. Degradation of nitrobenzene by Fenton-like reaction in a H₂O₂/schwertmannite system. *Chem. Eng. J.* **2016**, *283*, 873–879. [[CrossRef](#)]
10. Sun, Y.; Yang, Z.; Tian, P.; Sheng, Y.; Xu, J.; Han, Y.F. Oxidative degradation of nitrobenzene by a Fenton-like reaction with Fe-Cu bimetallic catalysts. *Appl. Catal. B Environ.* **2019**, *244*, 1–10. [[CrossRef](#)]
11. Elshafei, G.M.S.; Yehia, F.Z.; Dimitry, O.I.H.; Badawi, A.M.; Eshaq, G. Ultrasonic assisted-Fenton-like degradation of nitrobenzene at neutral pH using nanosized oxide of Fe and Cu. *Ultrason. Sonochem.* **2014**, *21*, 1358–1365. [[CrossRef](#)]
12. Anotai, J.; Sakulkittimasak, P.; Boonrattanakij, N.; Lu, M.C. Kinetics of nitrobenzene oxidation and iron crystallization in fluidized-bed Fenton process. *J. Hazard. Mater.* **2009**, *165*, 874–880. [[CrossRef](#)] [[PubMed](#)]
13. Ratanatamskul, C.; Chintitanun, S.; Masomboon, N.; Lu, M.C. Inhibitory effect of inorganic ions on nitrobenzene oxidation by fluidized-bed Fenton process. *J. Mol. Catal. A Chem.* **2010**, *331*, 101–105. [[CrossRef](#)]
14. Nitoi, I.; Oancea, P.; Raileanu, M.; Crisan, M.; Constantin, L.; Cristea, I. UV-VIS photocatalytic degradation of nitrobenzene from water using heavy metal doped titania. *J. Ind. Eng. Chem.* **2015**, *21*, 677–682. [[CrossRef](#)]
15. Shen, X.Z.; Liu, Z.C.; Xie, S.M.; Guo, J. Degradation of nitrobenzene using titania photocatalysts co-doped with nitrogen and cerium under visible light illumination. *J. Hazard. Mater.* **2009**, *162*, 1193–1198. [[CrossRef](#)]
16. Tayade, R.J.; Bajaj, H.C.; Jasra, R.V. Photocatalytic removal of organic contaminants from water exploiting tuned band gap photocatalysts. *Desalination* **2011**, *275*, 160–165. [[CrossRef](#)]
17. Weavers, L.K.; Liang, F.H.; Hoffmann, M.R. Aromatic compound degradation in water using a combination of sonolysis and ozonolysis. *Environ. Sci. Technol.* **1998**, *32*, 2727–2733. [[CrossRef](#)]
18. Zhao, L.; Ma, W.; Ma, J.; Wen, G.; Liu, Q. Relationship between acceleration of hydroxyl radical initiation and increase of multiple-ultrasonic field amount in the process of ultrasound catalytic ozonation for degradation of nitrobenzene in aqueous solution. *Ultrason. Sonochem.* **2015**, *22*, 198–204. [[CrossRef](#)]
19. Zhao, L.; Ma, J.; Sun, Z.Z.; Zhai, X.D. Catalytic ozonation for the degradation of nitrobenzene in aqueous solution by ceramic honeycomb-supported manganese. *Appl. Catal. B Environ.* **2008**, *83*, 256–264. [[CrossRef](#)]
20. Zhao, L.; Ma, J.; Sun, Z.Z.; Liu, H. Influencing mechanism of temperature on the degradation of nitrobenzene in aqueous solution by ceramic honeycomb catalytic ozonation. *J. Hazard. Mater.* **2009**, *167*, 1119–1125. [[CrossRef](#)]
21. Chen, Y.; Li, H.; Liu, W.; Tu, Y.; Zhang, Y.; Han, W.; Wang, L. Electrochemical degradation of nitrobenzene by anodic oxidation on the constructed TiO₂-NTs/SnO₂-Sb/PbO₂ electrode. *Chemosphere* **2014**, *113*, 48–55. [[CrossRef](#)]
22. Xia, K.; Xie, F.; Ma, Y. Degradation of nitrobenzene in aqueous solution by dual-pulse ultrasound enhanced electrochemical process. *Ultrason. Sonochem.* **2014**, *21*, 549–553. [[CrossRef](#)]
23. Ji, Y.; Shi, Y.; Wang, L.; Lu, J. Denitration and nitrification processes in sulfate radical-mediated degradation of nitrobenzene. *Chem. Eng. J.* **2017**, *315*, 591–597. [[CrossRef](#)]
24. Guo, J.; Zhu, L.; Sun, N.; Lan, Y. Degradation of nitrobenzene by sodium persulfate activated with zero-valent zinc in the presence of low frequency ultrasound. *J. Taiwan Inst. Chem. Eng.* **2017**, *78*, 137–143. [[CrossRef](#)]
25. Pan, Y.; Zhou, M.; Li, X.; Xu, L.; Tang, Z.; Sheng, X.; Li, B. Highly efficient persulfate oxidation process activated with pre-magnetization Fe⁰. *Chem. Eng. J.* **2017**, *318*, 50–56. [[CrossRef](#)]
26. Zhang, Y.; Xu, X.; Pan, Y.; Xu, L.; Zhou, M. Pre-magnetized Fe⁰ activated persulphate for the degradation of nitrobenzene in groundwater. *Sep. Purif. Technol.* **2019**, *212*, 555–562. [[CrossRef](#)]
27. De Luca, A.; He, X.; Dionysiou, D.D.; Dantas, R.F.; Esplugas, S. Effects of bromide on the degradation of organic contaminants with UV and Fe²⁺ activated persulfate. *Chem. Eng. J.* **2017**, *318*, 206–213. [[CrossRef](#)]
28. Chen, W.S.; Shih, Y.C. Mineralization of aniline in aqueous solution by sono-activated peroxydisulfate enhanced with PbO semiconductor. *Chemosphere* **2020**, *239*, 124686. [[CrossRef](#)]
29. Zheng, Z.; Huang, B.; Wang, Z.; Guo, M.; Qin, X.; Zhang, X.; Wang, P.; Dai, Y. Crystal faces of Cu₂O and their stabilities in photocatalytic reactions. *J. Phys. Chem. C* **2009**, *113*, 14448–14453. [[CrossRef](#)]

30. Su, Y.; Li, H.; Ma, H.; Robertson, J.; Nathan, A. Controlling surface termination and facet orientation in Cu₂O nanoparticles for high photocatalytic activity: A combined experimental and DFT study. *ACS Appl. Mater. Interfaces* **2017**, *9*, 8100–8106. [[CrossRef](#)]
31. Tang, H.; Liu, X.; Xiao, M.; Huang, Z.; Tan, X. Effect of particle size and morphology on surface thermodynamics and photocatalytic thermodynamics of nano-Cu₂O. *J. Environ. Chem. Eng.* **2017**, *5*, 4447–4453. [[CrossRef](#)]
32. Chu, C.Y.; Huang, M.H. Facet-dependent photocatalytic properties of Cu₂O crystals probed by electron, hole and radical scavengers. *J. Mater. Chem. A* **2017**, *5*, 15116–15123. [[CrossRef](#)]
33. Chen, W.S.; Huang, S.L. Photocatalytic degradation of bisphenol-A in aqueous solution by calcined PbO semiconductor irradiated with visible light. *Desalin. Water Treat.* **2020**, *190*, 147–155. [[CrossRef](#)]
34. He, S.L.; Wang, L.P.; Zhang, J.; Hou, M.F. Fenton pre-treatment of wastewater containing nitrobenzene using ORP for indicating the endpoint of reaction. *Procedia Earth Planet. Sci.* **2009**, *1*, 1268–1274. [[CrossRef](#)]
35. Satdeve, N.S.; Ugwekar, R.P.; Bhanvase, B.A. Ultrasound assisted preparation and characterization of Ag supported on ZnO nanoparticles for visible light degradation of methylene blue dye. *J. Mol. Liq.* **2019**, *291*, 111313. [[CrossRef](#)]
36. Chen, W.S.; Huang, C.P. Mineralization of aniline in aqueous solution by electro-activated persulfate oxidation enhanced with ultrasound. *Chem. Eng. J.* **2015**, *266*, 279–288. [[CrossRef](#)]
37. Liang, C.J.; Su, H.W. Identification of sulfate and hydroxyl radicals in thermally activated persulfate. *Ind. Eng. Chem. Res.* **2009**, *48*, 5558–5562. [[CrossRef](#)]
38. Lin, H.; Wu, J.; Zhang, H. Degradation of bisphenol A in aqueous solution by a novel electro/ Fe³⁺/ peroxydisulfate process. *Sep. Purif. Technol.* **2013**, *117*, 18–23. [[CrossRef](#)]
39. Wang, B.; Fu, T.; An, B.; Liu, Y. UV light-assisted persulfate activation by Cu⁰-Cu₂O for the degradation of sulfamerazine. *Sep. Purif. Technol.* **2020**, *251*, 117321. [[CrossRef](#)]
40. Xi, Q.; Gao, G.; Jin, M.; Zhang, Y.; Zhou, H.; Wu, C.; Zhao, Y.; Wang, L.; Guo, P.; Xu, J. Design of graphitic carbon nitride supported Ag-Cu₂O composites with hierarchical structures for enhanced photocatalytic properties. *Appl. Surf. Sci.* **2019**, *471*, 714–725. [[CrossRef](#)]
41. Sakar, M.; Balakumar, S. Reverse Ostwald ripening process induced dispersion of Cu₂O nanoparticles in silver-matrix and their interfacial mechanism mediated sunlight driven photocatalytic properties. *J. Photochem. Photobiol. A Chem.* **2018**, *356*, 150–158. [[CrossRef](#)]
42. Zhang, M.; Wang, J.; Wang, Y.; Zhang, J.; Han, X.; Chen, Y.; Wang, Y.; Karim, Z.; Hu, W.; Deng, Y. Promoting the charge separation and photoelectrocatalytic water reduction kinetics of Cu₂O nanowires via decorating dual-cocatalysts. *J. Mater. Sci. Technol.* **2021**, *62*, 119–127. [[CrossRef](#)]
43. Chen, L.; Guo, S.; Dong, L.; Zhang, F.; Gao, R.; Liu, Y.; Wang, Y.; Zhang, Y. SERS effect on the presence and absence of rGO for Ag@Cu₂O core-shell. *Mater. Sci. Semicond. Process.* **2019**, *91*, 290–295. [[CrossRef](#)]
44. Sharma, K.; Maiti, K.; Kim, N.H.; Hui, D.; Lee, J.H. Green synthesis of glucose-reduced graphene oxide supported Ag-Cu₂O nanocomposites for the enhanced visible-light photocatalytic activity. *Compos. Part. B* **2018**, *138*, 35–44. [[CrossRef](#)]
45. Biesinger, M.C.; Lau, L.W.M.; Gerson, A.R.; Smart, R.S.C. Resolving surface chemical states in XPS analysis of first row transition metals, oxides and hydroxides: Sc, Ti, V, Cu and Zn. *Appl. Surf. Sci.* **2010**, *257*, 887–898. [[CrossRef](#)]
46. Poulston, S.; Parlett, P.M.; Stone, P.; Bowker, M. Surface oxidation and reduction of CuO and Cu₂O studied using XPS and XAES. *Surf. Interface Anal.* **1996**, *24*, 811–820. [[CrossRef](#)]
47. Liu, S.; Zhao, X.; Zeng, H.; Wang, Y.; Qiao, M.; Guan, W. Enhancement of photoelectrocatalytic degradation of diclofenac with persulfate activated by Cu cathode. *Chem. Eng. J.* **2017**, *320*, 168–177. [[CrossRef](#)]
48. Liu, X.; Chen, J.; Liu, P.; Zhang, H.; Li, G.; An, T.; Zhao, H. Controlled growth of CuO/Cu₂O hollow microsphere composites as efficient visible-light-active photocatalysts. *Appl. Catal. A Gen.* **2016**, *521*, 34–41. [[CrossRef](#)]
49. Kumar, S.; Parlett, C.M.A.; Isaacs, M.A.; Jowett, D.V.; Douthwaite, R.E.; Cockett, M.C.R.; Lee, A.F. Facile synthesis of hierarchical Cu₂O nanocubes as visible light photocatalysts. *Appl. Catal. B Environ.* **2016**, *189*, 226–232. [[CrossRef](#)]
50. Anbu, P.; Gopinath, S.C.B.; Yun, H.S.; Lee, C.-G. Temperature-dependent green biosynthesis and characterization of silver nanoparticles using balloon flower plants and their antibacterial potential. *J. Mol. Struct.* **2019**, *1177*, 302–309. [[CrossRef](#)]
51. Han, Z.; Ren, L.; Cui, Z.; Chen, C.; Pan, H.; Chen, J. Ag/ZnO flower heterostructures as a visible-light driven photocatalyst via surface plasmon resonance. *Appl. Catal. B Environ.* **2012**, *126*, 298–305. [[CrossRef](#)]
52. Zhang, X.; Wang, Y.; Hou, F.; Li, H.; Yang, Y.; Zhang, X.; Yang, Y.; Wang, Y. Effects of Ag loading on structural and photocatalytic properties of flower-like ZnO microspheres. *Appl. Surf. Sci.* **2017**, *391*, 476–483. [[CrossRef](#)]
53. Maji, S.K.; Mukherjee, N.; Dutta, A.K.; Srivastava, D.N.; Paul, P.; Karmakar, B.; Mondal, A.; Adhikary, B. Deposition of nanocrystalline CuS thin film from a single precursor: Structural, optical and electrical properties. *Mater. Chem. Phys.* **2011**, *130*, 392–397. [[CrossRef](#)]
54. Štengl, V.; Grygar, T.M. The simplest way to Iodine-doped anatase for photocatalysts activated by visible light. *Int. J. Photoenergy* **2011**, *2011*, 685935. [[CrossRef](#)]
55. Kamaraj, E.; Somasundaram, S.; Balasubramani, K.; Eswaran, M.P.; Muthuramalingam, R.; Park, S. Facile fabrication of CuO-Pb₂O₃ nanophotocatalysts for efficient degradation of Rose Bengal dye under visible light irradiation. *Appl. Surf. Sci.* **2018**, *433*, 206–212. [[CrossRef](#)]

56. Muthukumar, M.; Niranjani, S.; Samuel Barnabas, K.; Narayanan, V.; Raju, T.; Venkatachalam, K. Green route synthesis and characterization of cuprous oxide (Cu₂O): Visible light irradiation photocatalytic activity of MB dye. *Mater. Today Proc.* **2019**, *14*, 563–568. [[CrossRef](#)]
57. Neta, P.; Huie, R.E.; Ross, A.B. Rate constants for reactions of inorganic radicals in aqueous solution. *J. Phys. Chem. Ref. Data* **1988**, *17*, 1027–1284. [[CrossRef](#)]
58. Hou, L.W.; Zhang, H.; Xue, X.F. Ultrasound enhanced heterogeneous activation of peroxydisulfate by magnetite catalyst for the degradation of tetracycline in water. *Sep. Purif. Technol.* **2012**, *84*, 147–152. [[CrossRef](#)]
59. Jyothi, K.P.; Yesodharan, S.; Yesodharan, E.P. Ultrasound (US), ultraviolet light (UV) and combination (US + UV) assisted semiconductor catalysed degradation of organic pollutants in water: Oscillation in the concentration of hydrogen peroxide formed in situ. *Ultrason. Sonochem.* **2014**, *21*, 1787–1796. [[CrossRef](#)] [[PubMed](#)]
60. Anipsitakis, G.P.; Dionysiou, D.D.; Gonzalez, M.A. Cobalt-mediated activation of peroxymonosulfate and sulfate radical attack on phenolic compounds Implications of chlorine ions. *Environ. Sci. Technol.* **2006**, *40*, 1000–1007. [[CrossRef](#)] [[PubMed](#)]
61. Zhou, J.; Xiao, J.; Xiao, D.; Guo, Y.; Fang, C.; Lou, X.; Wang, Z.; Liu, J. Transformations of chloro and nitro groups during the peroxymonosulfate-based oxidation of 4-chloro-2-nitrophenol. *Chem. Eng. J.* **2015**, *134*, 446–451. [[CrossRef](#)]